Instituto Tecnológico de Estudio Superiores de Monterrey

CAMPUS MONTERREY

Development of a Nanosatelite CubeSat 2U for the Monitoring of the Southern Return Circulation of the South

Members	Matrix
Eduardo Juárez Hernández	A01749005
Isaac Alexis López Paredes	A01747148
Juan Pablo Solis Ruiz	A01067387
Rubén Castillo Fernández	A01721993

Teachers:

Antonio Hernandez Gomez

Mauricio Alberto Garza Castañón

José Rodrigo Salmón Folgueras

Marvin Montoya Rangel

Claudia Bautista Flores

Francisco Montes

Luisa Fernanda Chaparro Sierra

Date

June 7, 2025

Table of Contents

Note: This document is an excerpt from the final report. The following table of contents lists only the sections included in this excerpt.

Chapter 6

Implemented subsystem: On-board antenna

6.1. Introduction

The communication system is critical in any satellite mission, as it allows both the sending of commands from ground stations and the reception of scientific data. One of the essential elements in this subsystem is the antenna, which is responsible for transmitting and receiving electromagnetic signals. In the case of CubeSats, the antenna design must ensure sufficient gain, good impedance match, and structural compatibility with the platform, all without employing complex deployment mechanisms. Table 6.1 summarizes the main design constraints.

In recent years, several types of antennas have been used in CubeSats, including monopoles, dipoles, helical and patch antennas. The latter have gained popularity as they can provide a considerable better gain (and consequently more data transmission) than dipole antennas. They are also lightweight, low-cost, easy to manufacture and do not require deployment mechanisms [58].

A patch antenna consists of a flat conductor on a dielectric substrate with a ground plane at its base. They commonly have a low bandwidth, however, there are ways to optimize their performance. One of them is using fractal geometry. A fractal is a recursively generated geometry that has fractional dimensions. Antennas with this structure make better use of the available area and have been proposed to operate on more than one frequency [60].

In this project, the design of a fractal patch in S-band is proposed, with double operating band, integrated with the CubeSat image acquisition system. This design seeks to meet the constraints imposed by the platform (Table 6.1) through a compact and lightweight design, the use of commercial materials and a flat geometry without deployment. In addition, critical variables such as the reflection coefficient, gain and thermal resistance are considered. This chapter describes the methodology followed, the simulations carried out, the design parameters selected, and finally, the results obtained.

Table 6.1: Antenna design constraints imposed by the CubeSat platform [14,58,59]

.

Restriction	Description
Size and Dough	Lightweight and compact to fit the surface of a 10 cm CubeSat × 10 cm in the case of 1U.

Deployment	The deployment mechanism should be chosen or designed to minimize the risk of deployment failure.
Frequency Band and Bandwidth	Established by the specifications of the mission and assigned by the International Telecommunication Union.
Reflection coefficient $S11$	Less than -10 dB.
Profit	It must be at least 2 dB in S-band.
Link Margin	Greater than 6 dB to ensure reliable communication.
Space Environment and Durability	Resist thermal variations from -40 to +85 degrees Celsius. It must pass vacuum thermal cycling and vibration tests.
Cost	Use of commercial materials to reduce the budget.
Polarisation	Circular polarization to reduce losses due to polarization misalignment. The axial ratio must be less than 3 dB.

6.2. Design methodology

6.2.1. Justification

The main objective of the mission is to observe the Southern Southern Overturning Circulation (GCOS) using infrared sensors in a 2U CubeSat on a synchronous solar orbit, with an altitude of 650 km and an inclination of 97°. As shown in Table 6.1, the antenna should have a minimum gain of 2 dB, a reflection coefficient $S11$ of less than -10 dB, and should respect the geometric constraints of 100 mm x 100 mm x h. In addition, circular polarization is required to maximize the efficiency of the downlink with the ground station.

Due to the nature of the mission, the useful load requires continuous observation of the ocean. This configuration can be used to use directional antennas and therefore require less power without compromising the performance of the communication link [61]. Patch antennas are an ideal solution for this purpose. In addition, by using fractal geometry it is possible to obtain an antenna with two resonant frequencies, one for reception and one for transmission, while maintaining a small area and an aperture for usable loading. With this it is possible to use the same face for the antenna and the observation system, optimizing space and leaving more faces available for solar panels. Finally, the use of deployable antennas or additional systems is avoided, which helps to reduce the risk of failures in mobile mechanisms [58].

On the other hand, the choice to operate in the S-band (2-4 GHz) is justified by regulatory considerations and scientific reasons. This band is allocated to satellite services for space operation (2025–2110 MHz), space research (2200–2290 MHz) and amateur satellite services (2400–2450 MHz) [62]. For a mission focused on observing GCOS with high-resolution images, large data volumes are required. The S-band allows high-bit-rate links to be established with ground stations without increasing the size and weight of the antenna. In addition, due to the characteristics of the operating orbit (LEO-SSO), the contact time with the station is limited [48]. Therefore, the S-band is a viable option to transmit data at a higher speed than the

traditional VHF/UHF (very high frequency and ultra high frequency) bands, while remaining more accessible than more complex and expensive bands such as the X band [58].

The substrate selection process, design parameters and fractal geometry of the proposed patch antenna are detailed below.

6.2.2. Substrate selection

The diel that was selected for the design of the patch antenna was FR4, a laminate of fiberglass woven with an epoxy resin binder [63]. This decision was made based on its balance between cost, ease of manufacture and performance in prototyping stages. This material, widely used in printed circuit board (PCB) technologies, offers a relative permittivity of $\varepsilon r \sim 4.3$, Loss tangent $\tan\delta \sim 0.02$ and thickness h = 1.6 mm [64]. Techniques such as the use of air spacers and layer overlapping mitigate their diel-electric losses, achieving gains of up to 25.6 dB in 8 × 8 arrays [64].

However, its thermal degradation above $300 \circ C$ [65] limits its applicability in extreme space environments. For advanced missions, materials such as Rogers RT/duroid© [61] are more suitable due to their lower $\tan\delta$ (~ 0.0012) and radiation stability.

Some key advantages that the FR4 has are:

- Reduced cost: Ideal for prototypes, where optimization requires multiple iterations [14].
- PCB integration: Compatibility with standard techniques (chemical etching, microstrip), facilitating the manufacture of multiband geometries [66].
- Adaptability: Allows adjusting dielectric layers or spacers to optimize bandwidth and gain [64].
- Mechanical robustness: Resistance to vibrations during casting and moderate humidity [65].

On the other hand, although FR4 is optimal for conceptual validation, its performance in the field is compromised by:

- Electrical losses: Reduce radiant efficiency in high-power applications.
- Frequency dependence: εr_{eff} varies quadratically with frequency ($\varepsilon r_{eff} \propto f2$), requiring compensation in multiband designs [66].
- Chemical degradation: The release of volatile compounds under vacuum [65].

For critical missions, it is recommended to transition to substrates such as Rogers RT/duroid© 5870, which maintain dielectric stability ($\Delta\varepsilon r < 0.05$) in ranges from $-55 \circ C$ to $125 \circ C$ [61].

6.2.3. Design parameters

Once the substrate was chosen, the resonance frequency of the fr antenna was defined at 2.45 GHz. This gives the W width of the radiator head [60]:

$$W = \frac{c}{f_r \sqrt{\frac{\epsilon_r + 1}{2}}} \tag{6.1}$$

where c is the speed of light in a vacuum and εr is the relative dielectric permittivity of the substrate. The procedure detailed in [14] for constructing an anisotropic Zhanbanev fractal is now followed. As shown in Figure 6.1, you start with a square of dimensions $W = 2\mathrm{L}$. Then, a cut of a square is made in the center with sides of length L. Now, the fractal is formed depending on the desired hierarchical order . In our case ($n = 1$), the antenna will have two square patches of effective length $L1$ and $L2$, which would result in two operating frequencies. $L2$ is obtained with:

$$L_2 = \sqrt{2}\left(\frac{1}{2} + \sum_{n=1}^{N}\left(\frac{1}{3^n}\right)\right) L_1 \tag{6.2}$$

Therefore the sides of the square fractals of the first level have as dimensions $H = L/3$.

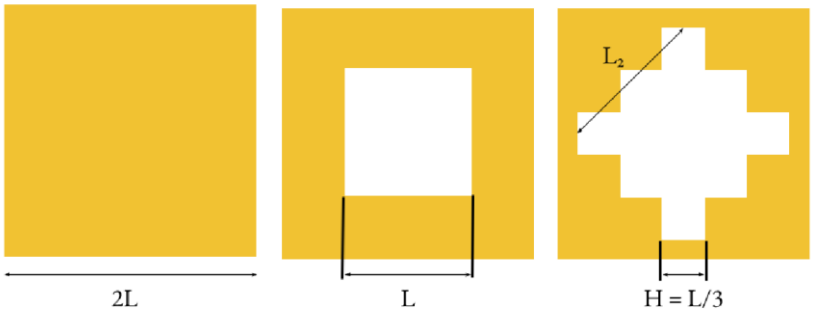

Figure 6.1: Formation of the antenna radiator patch according to the hierarchical formation of anisotro'pico fractal.

To integrate with the image acquisition system, the antenna has a circular hole of diameter $d = 36$ mm. It was determined that the antenna would be placed on one of the side faces. To be compatible with the rails and to be able to fit the structure, the overall dimensions of the antenna are 84 mm x 108 mm.

Finally, the power point from the centre of the antenna is (31.33) mm. A female SMA connector was used as the port. The final antenna design is shown in Figure 6.2 and Table 6.2 summarizes the design parameters.

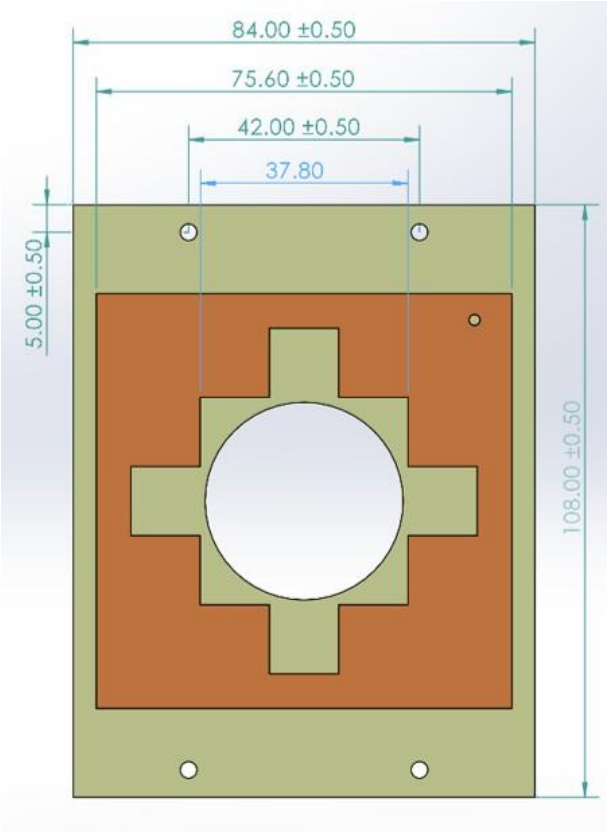

Figure 6.2: 2D model of the antenna

Table 6.2: Fractal antenna design parameters

Torque	Value (mm)
L	37.8
2L	75.6
d	36
L1	37.8
L2	44.548
h	1.6
H	12.6

6.3. Electromagnetic simulation

To validate the expected performance of the design, simulations were carried out using the High Frequency Structure Simulator (HFSS) of ANSYS Electronics. Figure 6.3 shows the reflection coefficient $S11$, which represents the proportion of energy reflected at the antenna input port [60]. A value below –10 dB indicates good impedance matching, ensuring that most of the power is efficiently transferred into the clearance. It is observed that the antenna has

resonance frequencies at 2.45 GHz and 2.06 GHz, with $S11$ values less than –10 dB. The corresponding bandwidths were 72 MHz and 45 MHz, respectively.

Figure 6.4 shows a gain of –1.07 dB for the 2.45 GHz frequency. Gain is a measure of the antenna's ability to concentrate radiated energy in a specific direction, compared to an isotypical antenna [60]. Although this value is not suitable for space applications, it is sufficient as a starting point for a first prototype. To improve gain, it is suggested to increase the thickness of the substrate by stacking several layers, as shown in [14]. Alternatively, an optimised design with improved electromagnetic performance is presented in section 6.5.

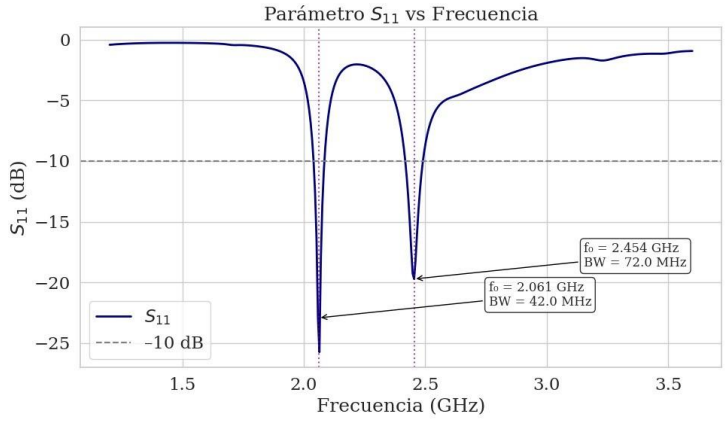

Figure 6.3: Simulated $S11$ reflection coefficient for the antenna implemented as a prototype with FR4 substrate. The two resonance frequencies and their respective bandwidth are displayed

6.4. Implementation and validation of the prototype

To implement and validate a functional prototype of the system, low-cost and easy-to-acquire electronic components were selected. A future iteration envisages replacing these elements with versions specifically designed to operate in the space environment. This is detailed in section 6.5 below.

Table 6.3 summarizes the components used. The antenna PCB is designed in KiCad electronic design software. Later it was manufactured on an FR4 substrate in a ProtoMat S63 machine in the micro robotics laboratory at the Tecnológico de Monterrey Campus Monterrey, with the help of doctoral student Daniel Hugo Solano Ter'an. The prototype can be visualized in Figure 6.5 along with the test communications system. This is based on a 2.4 GHz transceiver (transmission and reception device) controlled by a Raspberry Pi Zero 2W. The antenna is connected to the transceiver by means of a 50 ohm coaxial line. Figure 6.6 shows these connections.

The radiofrequency module used was E01-ML01DP5 [67]. This device incorporates an nRF24L01 transceiver [68] with a power amplifier (PA) and a low-noise amplifier (LNA). It operates in the international ISM (Industrial, Scientific and Medical) band of

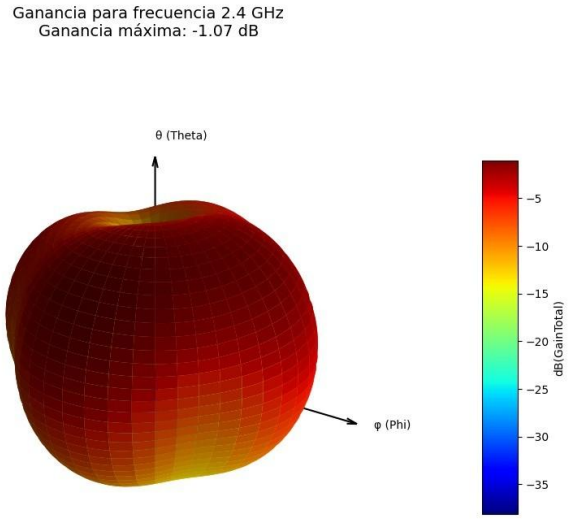

Figure 6.4: Simulated radiation pattern for the FR4 antenna prototype. A maximum gain of -1 dB is shown for the transmission frequency (2.4 GHz).

2.4–2.525 GHz. Operates at 3.3 V, with an operating temperature range of –40 °C to 85 °C. Its maximum transmission power is 20 dBm, with a typical consumption of 130 mA, while in reception, the consumption is 20 mA. It features a sensitivity of –96 dBm at 250 kbps and supports data rates of 2 Mbps, 1 Mbps, and 250 kbps. It has a 50 ohm SMA connector.

Once the system was assembled, communication tests were carried out with another transceiver. Stable transmission was achieved at a distance of 85 m. Test images as well as images taken by infrared sensors were transmitted MLX90640ESF at a rate of 250 kbps. Telecommands from another antenna were also successfully received.

Table 6.3: Electronic components for prototype implementation.

Component	Model	Datasheet
PCB Antenna Substrate	FR4	[63]
2.4 GHz Transceiver	E01-ML01DP5 (nRF24L01P+PA+LNA)	[67]
Raspberry Pi 0	RPIZero2WH	[69]
Coaxial transmission line	RG316 with SMA connector	N/A

Finally, as part of the experimental validation of the prototype, an FR4 plate and an nRF24L01 module were vacuum-tested. The procedure is described in Chapter 7. At the end of the test, no structural failures were observed, which helps to have a first mechanical validation. However, the antenna also needs to be subjected to thermal and vibration tests, as well as tests to characterise the electromagnetic parameters of the antenna. As future work, it is important to measure the radiation pattern, gain and reflection coefficient to validate the results of the simulations.

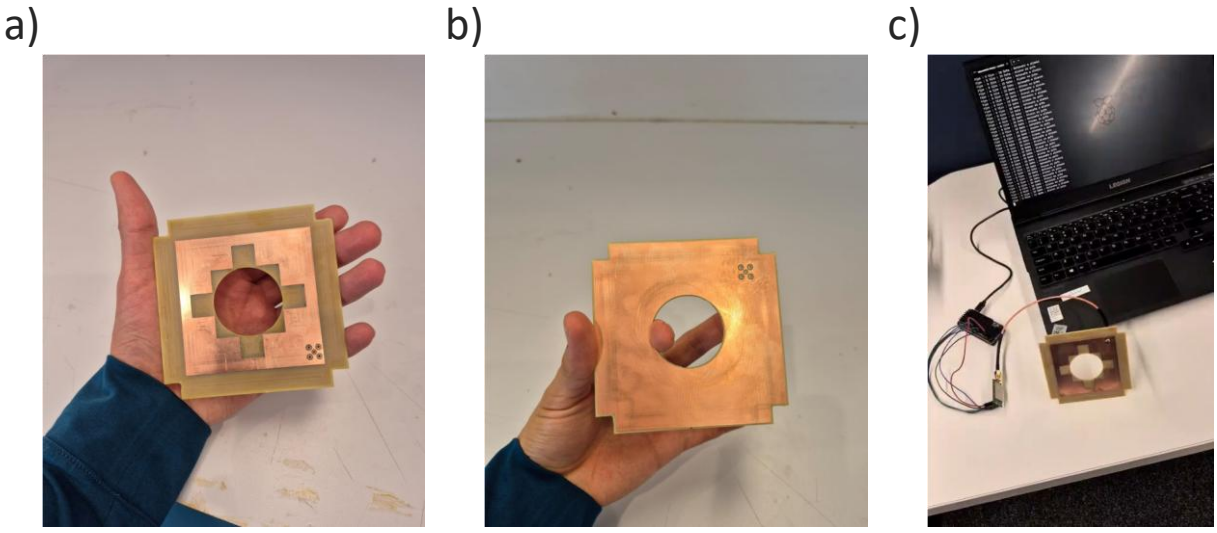

Figure 6.5: a) Front view of the antenna (radiator patch), b) Rear view (Earth), C) Test configuration of the prototype.

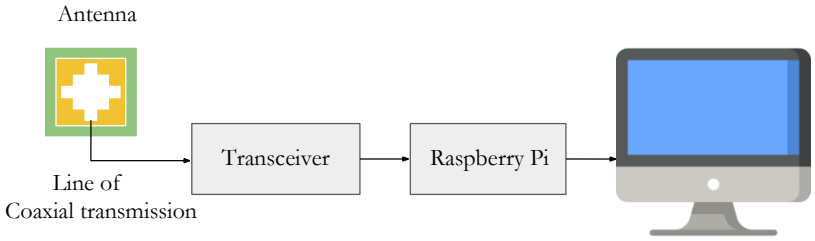

Figure 6.6: Configuration for validation of the implemented communication prototype

6.5. Proposed communications system

In order to strengthen the communications system for operation in orbit, a new configuration based on certified components and a redesign of the patch antenna is proposed. The aim is to propose a complete system that meets the efficiency and reliability objectives required by the objectives of the GCOS observation mission.

During the development of the initial prototype, the nRF24L01 module was used as the only transceiver operating on a single frequency within the ISM band for reasons of simplicity and commercial availability. However, in an orbit mission, it is recommended to separate the transmit (Tx) and receive (Rx) frequencies within the S-band, e.g. Tx at 2200-2290 MHz and Rx at 2025-2110 MHz, in order to avoid interference between channels, to allow simultaneous operation (full-duplex), and to comply with spatial communication standards [62, 70].

6.5.1. Selected components

Transceiver

EnduroSat's S-Band Transceiver *($14,000 USD), designed specifically for CubeSat missions and tested in orbit [*71], was selected. This transceiver operates on two independent channels for

Tx and Rx: 2200-2290 MHz and 2025-2110 MHz respectively. It has an output power of 26 dBm to 33 dBm (0.3 W - 2 W) and modulation compatible with the standard CCSDS protocol.

Diplexer

To physically separate the Tx and Rx channels, the Wiran *S-Band Diplexer*, also tested in the field, is incorporated. This component has two ports: for Tx on 2200-2290 and for Rx on 2025-2110 MHz [72]. It offers an insertion loss of 1 dB and isolation greater than 75 dB to ensure that the Tx signal does not interfere with the Rx signal. Its design also makes it suitable for direct integration with the communications subsystem.

Redesign of the radiator patch

To ensure compatibility with the frequencies of the selected components, as well as to improve radiation efficiency and stability in space conditions, it is proposed to redesign the patch antenna on the RT/duroid© 6006 substrate. This material has a high relative permittivity $\varepsilon r = 6.15$, which allows the resonance frequencies to be reduced without increasing the physical size of the head, which is crucial to keep the system compact. In addition, its low tangent loss ($\tan\delta = 0.0019$) and its thermal properties make it suitable for space applications, where extreme variations in temperature and radiation exposure can affect conventional materials such as FR4 [73].

With this new material, the dimensions of the fractal patch must be adjusted to the new εr value and the resonant frequencies of 2.23 and 2.06 GHz that support the transcator and diplexer. However, it is possible to maintain geometric constraints, including the 36 mm central opening for the optical system and the side cuts to integrate with the rails of the structure. Figures 6.7 and 6.8 show the simulations for antenna redesign. The resonant frequencies were 2230 MHz and 2066 MHz with $L = 36.03\text{mm}$ and the feed in (27.29) mm. The gain for the Tx frequency was 2.86 dB, a considerable improvement over the antenna in FR4.

Integration and compatibility

In conclusion, this new configuration (Figure 6.9) allows for a more reliable and application-oriented communications system in a complete communications system for CubeSats, especially those requiring the transmission of large volumes of data on observation missions such as the one in this project. The proposed system has the following advantages:

- High energy efficiency with low consumption and high gain components.
- Support for standardized CCSDS links
- Structural and thermal reliability with RT/duroid© 6006
- Simultaneous Tx/Rx operation capability thanks to the specialized web diplexer

S

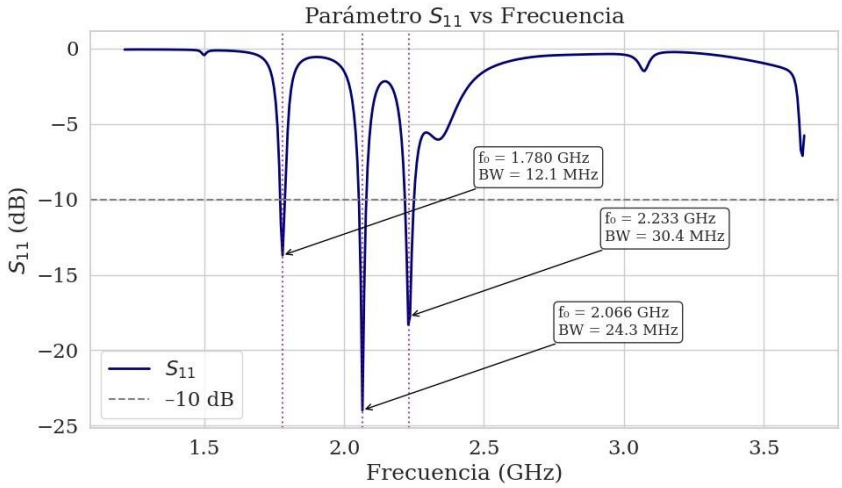

Figure 6.7: Simulated *S11* reflection pattern for the antenna implemented as a prototype with Rogers RT duroid 6006 substrate. The two resonance frequencies and their respective bandwidth are displayed

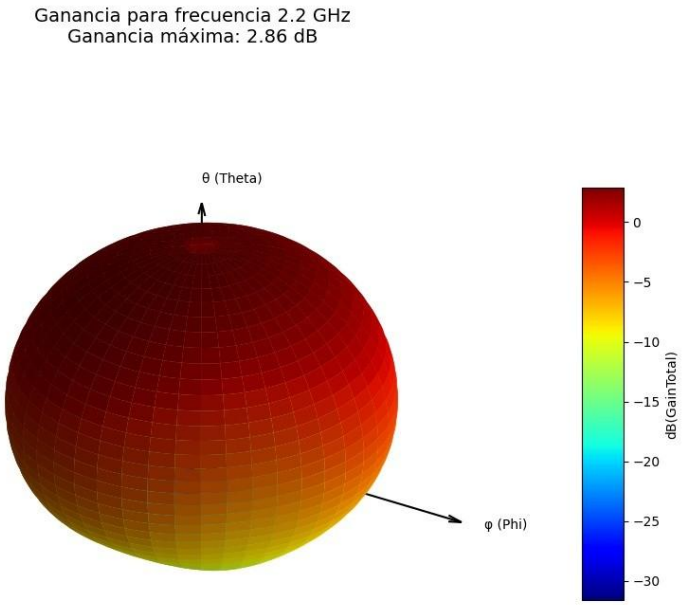

Figure 6.8: Simulated radiation pattern for the antenna with Rogers RT/duroid© 6006. A maximum gain of 2.86 dB is shown for the Tx frequency (2.23 GHz).

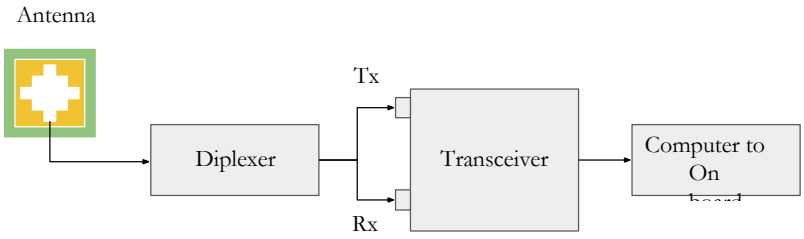

Figure 6.9: Configuration of the proposed ideal communications system. The antenna will be manufactured on a Rogers RT/duroid© 6006 substrate and commercial components are proposed for the transceiver and diplexer [71,72].

6.5.2. Link Budget

From this communications system, a link budget analysis was carried out with functions of the MATLAB *Satellite Communications Toolbox*. This is in order to assess the feasibility of communication between the elite satellite and the land station. First, the access intervals are calculated, using the orbital elements shown in Table 5.2 and the geographical location of the station as input. The simulation assessed, in discrete time steps, whether there was a line of sight and whether the elevation of the elite sat exceeded 5°, in line with what was reported in [57]. The results made it possible to identify communication windows over a period of 7 days. As a result, an orbital period of 97.7 minutes and an average access time of about 28 minutes was obtained, with 4 stops per day. Considering a data rate of 250 kbps, there would be a maximum transmission capacity of 58 MB per day.

The bond margin was then calculated, which is defined as the difference between the $Eb/N0$ (energy-per-bit ratio to noise spectral density) received and the minimum $Eb/N0$ required for communication to be successful. This margin represents how much reserve the system has against additional losses not considered (such as interference, atmospheric attenuation or variations in the attitude of the sat elite). In general, a positive margin indicates that the system has sufficient capacity to maintain reliable communication; while a low or negative margin suggests a risk of link failure [74]. In particular, a margin of at least 6 dB is recommended for a reliable communication system on CubeSats [75].

For this analysis, the hardware parameters of the proposed communications system shown in Table 6.4 are considered. A communications system with a 2.06 GHz uplink and a 2.23 GHz downlink from the station to the station is envisaged, both within the range assigned to the S-band. The antenna uses the fractal patch design with the Rogers plate, which has a simulated gain of 3 dB.

On board the sat´elite, the EnduroSat S-band transceiver is used, which allows a maximum transmission power of 33 dBm (compared to 20 dbm in the NRF24L01) and is compatible with the standard CCSDS (Consultative Committee for Space Data Systems) coding [71]. For the sat'elite receiver, an estimated sensitivity of –100 dBm is considered for a data rate of 125 kbps and a gain/noise temperature (G/T) ratio of –21.2 dB/K, consistent with what was reported in [75].

At the ground station located in Monterrey, a satellite dish of 2 meters in diameter is configured, with an estimated gain of 28 dBi, transmitting at 20 dBW (100 W) of power. The terrestrial receiver has a G/T of 6.8 dB/K, a reasonable value for university or semi-professional stations, and also in accordance with the literature [75].

System losses in both the elite and ground stations are set to the default conservative value of 5 dB according to the MATLAB tool. These include losses from connectors, cables, filters, misalignments, and thermal effects. Finally, a required ($Eb/N0$) of 10 dB is considered, typical for CCSDS links with a low error rate [75]. As shown in Figure 6.10, for both links there is a link greater than 6 dB during the 2-day access windows, which indicates a high reliability of the proposed system.

Table 6.4: Parameters used for the analysis of the Link Budget of the CubeSat communications system. The values considered for both *uplink* (transmission from the terrestrial station to the sat elite) and downlink (transmission from the sat elite to the terrestrial station) are presented.

Torque	Unity	Uplink	Downlink
Frequency	GHz	2.06	2.23
Transmission power	dBW	20	3
Data rate	Mbps	0.125	0.125
Tx antenna gain	dBi	28	3
Rx antenna gain	dBi	3	28
G/T receiver	dB/K	–21.2	6.8
$Eb/N0$ required	dB	10	10

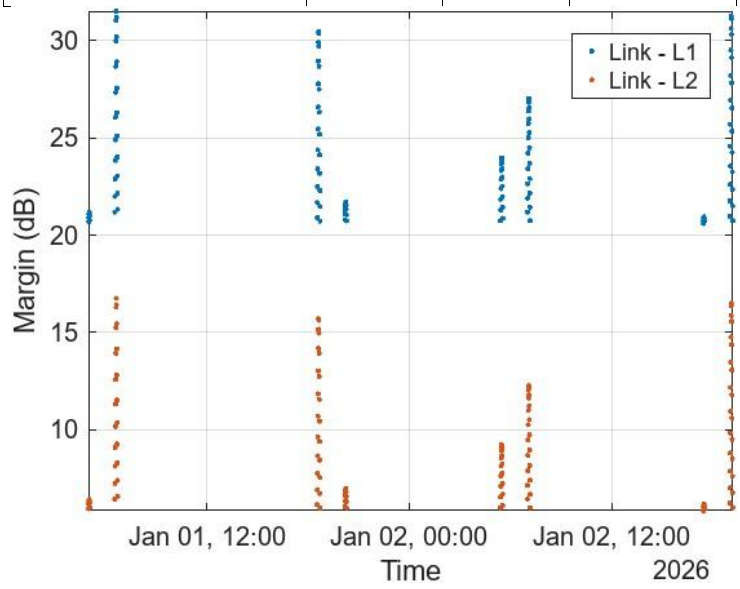

Figure 6.10: Link margin calculated for the CubeSat communication system considering the operating conditions in the selected area. L1 is the link from the terrestrial station to the

satellite and L2 from the satellite to the station. The analysis was performed in MATLAB using the visibility windows over a period of 2 days. 5.2.

6.6. Conclusions and recommendations

This work allowed the development and validation of a functional prototype of a fractal patch antenna for use on board a CubeSat focused on monitoring GCOS. The design allows the use of two operating frequencies in the S-band, ideal for the transmission with high data rate that requires continuous observation of the Southern Ocean. In addition, its compact and lightweight design minimizes risks due to deployment mechanisms and optimizes space by sharing a face with the optical system.

Using a commercial transceiver NRF24L01 operating in the 2.4 GHz band, the effectiveness of the antenna manufactured on an FR4 substrate was verified, verifying both its mechanical integration and its electromagnetic performance. Experimental tests were carried out, including simulation of the reflection coefficient ($S11$) and gain, as well as the successful establishment of a data link between two modules separated by a distance of 85 m. In addition, tests were carried out under vacuum conditions without any structural failures in the antenna or connections, which supports the physical integrity of the system under conditions similar to those of orbital operation.

At the same time, a proposal was developed for the communications system which would enable it to be implemented in a real mission. This includes the use of a certified transceiver for space applications, the EnduroSat S-Band Transceiver, and a WiRan diplexer, specifically designed for S-band operation with separate frequencies for transmission (2200–2290 MHz) and reception (2025–2110 MHz). In addition, the antenna is designed on an advanced RT/duroid© 6006 substrate, whose high permittivity and low electrical loss offer superior electromagnetic performance (simulated gain of 2.85 dB) and greater thermal stability, meeting the requirements of the space environment.

In addition, a link budget analysis was carried out considering the selected area and the proposed components, which allowed the calculation of the expected link margin for the system. The result was a margin of 6 dB, indicating sufficient reserve to compensate for unmodeled losses and ensure reliable communication during orbital access windows.

As a main recommendation, it is proposed to carry out physical characterization tests of the antenna to validate the results obtained in simulation. This includes the measurement of the reflection coefficient ($S11$), radiation standard and gain in the laboratory, as well as tests of thermal durability and mechanical strength. In addition, integration with a more robust and certified transceiver system for space environments will also be essential to assess its actual performance in mission. These actions would make it possible to bridge the gap between the theoretical model and actual performance, facilitating its effective incorporation into the complete CubeSat system.

Chapter 7

On-board antenna vacuum tests

7.1. Procedure

This section describes the vacuum tests of the components used for the prototype of the antenna system on board the CubeSat. The tests were carried out at Busch Vaccum Solutions. This component, described in Chapter 6, is crucial for communication between the elite satellite and the ground station, both for receiving commands and for transmitting the scientific data collected during the mission. Figure 7.1 shows the tested components: an FR4 PCB board on which a NRF24L01 radio frequency module, an SMA connector, and a capacitor were soldered. The final prototype was not used but the same materials and components were used, so its structural performance can be evaluated.

A test was carried out in a medium vacuum and another in a high vacuum. A HiScroll 46 pump was first used for this purpose. This first phase 1 lasted 5 and a half minutes and reached up to $10{-}2$ mbar. For the second phase, a HiPace® 80 turbomolecular pump was used together with the first pump. In this way, up to $10{-}5$ mbar was reached after 7 minutes and 21 seconds. The pump specifications are summarized in Table 7.1

(a) After the half-empty test.

(b) After the high vacuum test

Figure 7.1: On-board antenna components in the vacuum chamber. A printed circuit board in FR4, a radio frequency module, an SMA connector and a capacitor are shown.

(a) HiScroll 46 scroll pump

(b) HiPace® 80 Turbomolecular Pump

Figure 7.2: Vacuum pumps used to perform the tests.

Table 7.1: Key characteristics of the HiPace® 80 Neo and HiScroll 46 pumps for vacuum testing.

Characteristics	HiPace® 80 Neo (Turbomolecular)	HiScroll 46 (Scroll)
Pump Type	Turbomolecular	Scroll (dry, oil-free)
Pumping speed	N2: 67 l/s	43 m3/h (~ 11.944 l/min)
Minimum achievable pressure	Not directly specified (high compression)	7 × 10-3 hPa
Input Voltage	24 V DC (±10%)	100–127 / 200–240 V AC (±10%)
Maximum power consumption	110 W	Not directly specified

7.2. Results

Figures 7.3a and 7.3b show the behavior of pressure with respect to time inside the vacuum chamber. The curves were obtained by manually recording the pressure every second.

During Phase 2 (Figure 7.3b) an initial continuous decrease in pressure was observed to approximately $10{-}3$ mbar, followed by a region of oscillations, where pressure does not decrease in a sustained manner and shows instability, with values fluctuating between $10{-}4$ mbar and $10{-}3$ mbar. This behavior contrasts with Phase 1, where pressure decreases continuously and without significant oscillations (Figure 7.3a).

Both FR4 and NRF24L01 are components that can release gases under vacuum conditions (*outgassing* [76]), which could explain the fluctuations observed in pressure during Phase 2. The FR4 material, made from epoxy resin and fiberglass, absorbs moisture from the environment and then releases it into the vacuum. Similarly, the components of the NRF24L01 module, such as plastic encapsulates and resins, can also contribute to the detachment of volatile compounds.

This interpretation is supported by the study by Scheuer et al. [76], where outgassing *rates were measured* for several types of FR4 laminates after irradiation. The authors report that even with moderate pre-bake (50°C), *outgassing rates*

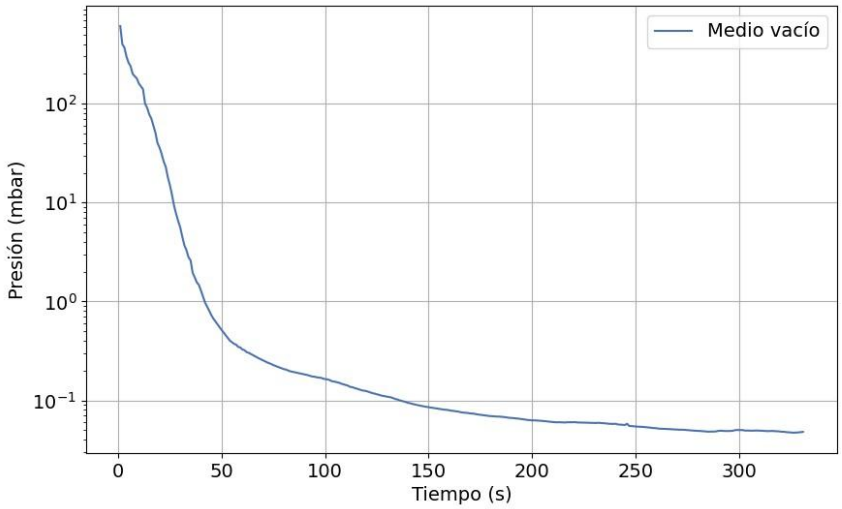

(a) Phase 1

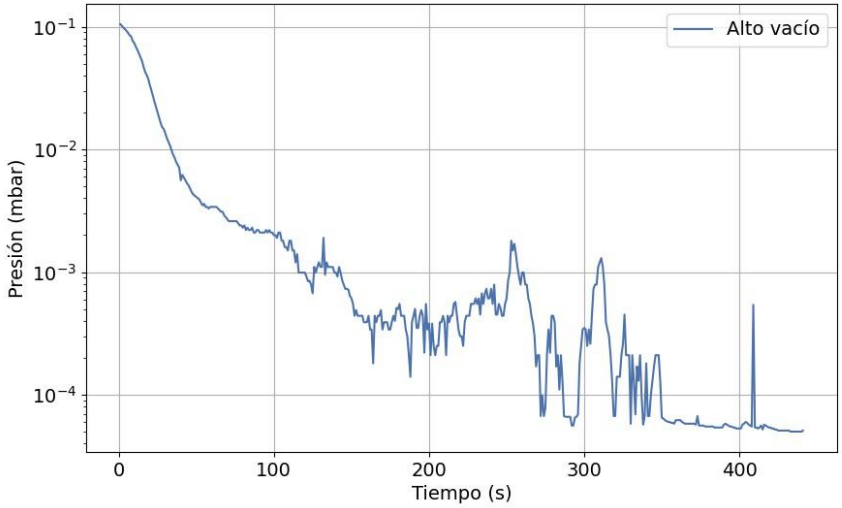

(b) Phase 2

Figure 7.3: Pressure against time in the vacuum chamber. (a) In phase 1, up to 4 were reached.$8 \times 10{-}2$ mbar for 5 minutes, b) In phase 2 it was reached up to $5 \times 10{-}5$ mbar for 7 minutes.

in FR4 they remain in the order of $10{-}8$ torr·L·s−1·cm−2. In addition, it was observed that substrates with higher resin content (such as those with low or medium TG) have a greater propensity to desorb gases under vacuum, compared to special laminates such as Rogers, which had practically zero *outgassing* rates under similar conditions.

In space applications, this type of behavior can be critical, as gases can condense into sensitive optical, thermal, or electrical components, affecting the functionality and reliability of the on-board system. Therefore, *bake-out* is recommended, as suggested by comparative studies of compatibility with ultra-high vacuum [76]. Another alternative is to use specialized laminates

such as the Rogers RT duroid 6006 proposed in this project to manufacture the antenna (section 6.5).

It is worth mentioning that, after the test, no visible structural failures or deformations were observed in the PCB or in the NRF24L01 module (Figure 7.1), suggesting that, despite the release of gases, the components maintain their mechanical integrity under vacuum conditions. However, because the final prototype was not tested, it was not possible to test whether the antenna was capable of transmitting after being idle. As future work, this test would help confirm the viability of the system in the space environment.

[47] H. Al-Hraishawi, H. Chougrani, S. Kisseleff, E. Lagunas, and S. Chatzinotas, "A Survey on Nongeostationary Satellite Systems: The Communication Perspective," *IEEE Communications Surveys & Tutorials*, vol. 25, no. 1, pp. 101–132, 2023.

[48] C. Nieto-Peroy and M. R. Emami, "CubeSat Mission: From Design to Operation," *Applied Sciences*, vol. 9, p. 3110, Aug. 2019. Publisher: MDPI AG.

[49] ESA, "Types of orbits." https://www.esa.int/Enabling_Support/Space_Transportation/Types_of_orbits#PO, Mar. 2020. Accessed: May 23, 2025.

[50] CSIS, "Popular Orbits 101." https://aerospace.csis.org/aerospace101/ earth-orbit-101/, 2017. Accessed: May 24, 2025.

[51] Z. Yang, P. Zhang, S. Gu, X. Hu, S. Tang, L. Yang, N. Xu, Z. Zhen, L. Wang, Q. Wu, F. Dou, R. Liu, X. Wu, L. Zhu, L. Zhang, S. Wang, Y. Sun, and W. Bai, "Capability of Fengyun-3D Satellite in Earth System Observation," *Journal of Meteorological Research*, vol. 33, pp. 1113–1130, Dec. 2019.

[52] E. Haas, D. Moyer, and F. Luccia, "J14.5 MAINTAINING SNPP VIIRS REFLECTIVE SOLAR BAND SENSOR DATA RECORD QUALITY: ON-ORBIT UPDATE OF SCREEN TRANSMISSION AND SOLAR DIFFUSER BRDF PARAMERS," 2015.

[53] Y. Zhang, Y. Xu, and H. Zhou, *Theory and Design Methods of Special Space Orbits*. Singapore: Springer Singapore, 2017.

[54] W. Lv, P. Yang, Y. Ding, Z. Wang, C. Lin, and Q. Wang, "Energy-Efficient and QoSAware Computation Offloading in GEO/LEO Hybrid Satellite Networks," *Remote. Sens.*, vol. 15, p. 3299, June 2023.

[55] G. Tzanoulinos, N. Ait-Mohammed, and V. Lappas, "Design of CubeSat-Based MultiRegional Positioning Navigation and Timing System in Low Earth Orbit," *Aerospace*, Dec. 2024.

[56] J. Matar, M. Rodŕ ıguez-Cassola, G. Krieger, P. Lo'pez-Dekker, and A. Moreira, "MEO SAR: System Concepts and Analysis," *IEEE Transactions on Geoscience and Remote Sensing*, vol. 58, pp. 1313–1324, Feb. 2020.

[57] M. A. El Moukalafe and K. Minaoui, "Communication Optimization Approach for SBand LEO CubeSat Link Budget," in *WITS 2020* (S. Bennani, Y. Lakhrissi, G. Khaissidi, A. Mansouri, and Y. Khamlichi, eds.), vol. 745, pp. 1001–1011, Singapore: Springer Singapore, 2022. Series Title: Lecture Notes in Electrical Engineering.

[58] S. Liu, P. I. Theoharis, R. Raad, F. Tubbal, A. Theoharis, S. Iranmanesh, S. Abulgasem, M. U. A. Khan, and L. Matekovits, "A Survey on CubeSat Missions and Their Antenna Designs," *Electronics*, vol. 11, p. 2021, Jan. 2022. Number: 13 Publisher: Multidisciplinary Digital Publishing Institute.

[59] H. H. Abdullah, A. Elboushi, A. E. Gohar, and E. A. Abdallah, "An Improved S-Band CubeSat Communication Subsystem Design and Implementation," *IEEE Access*, vol. 9, pp. 45123–45136, 2021.

[60] C. A. Balanis, *Antenna Theory: Analysis and Design*. John Wiley & Sons, Feb. 2016. Google-Books-ID: iFEBCgAAQBAJ.

[61] A. Nascetti, E. Pittella, P. Teofilatto, and S. Pisa, "High-gain s-band patch antenna system for earth-observation cubesat satellites," *IEEE Antennas and Wireless Propagation Letters*, 2015.

[62] E. National Academies of Sciences and Medicine, *Handbook of Frequency Allocations and Spectrum Protection for Scientific Uses: Second Edition*. Washington, DC: The National Academies Press, 2015.

[63] Laminated Plastics, *Technical Data Sheet FR-4*. Available in https:// laminatedplastics.com/fr-4.pdf.

[64] B. Honarbakhsh, "High-gain low-cost microstrip antennas and arrays based on fr4 epoxy," *Int. J. Electron. Commun. (AEU)",* vol. 75, pp. 1–7, 2017.

[65] C. F. Rodrigues, L. Blaga, and B. Klusemann, "Friction riveting of fr4 substrates for printed circuit boards: Influence of process parameters on process temperature development and joint properties," *Journal of Materials Research and Technology*, vol. 24, pp. 4639–4649, 2023.

[66] J. Paleˇcek, M. Vestenick´y, P. Vestenick´y, and J. Spalek, "Frequency dependence examination of pcb material fr4 relative permittivity," in *12th IFAC Conference on Programmable Devices and Embedded Systems*, pp. 90–94, 2013.

[67] Chengdu Ebyte Electronic Technology, *E01-ML01DP5 User Manual*, 3 2025. Rev. 1.6. Available on https://www.es-ebyte.com/products/E01-ML01DP5/4#Downloads.

[68] Nordic Semiconductor, *nRF24L01 Single Chip 2.4GHz Transceiver. Product Specification*, 2007. Rev. 2.0. Available in https://cdn.sparkfun.com/datasheets/Wireless/Nordic/nRF24L01_Product_Specification_v2_0.pdf.

[69] Raspberry Pi Ltd, *Raspberry Pi Zero 2 W*, 4 2014. Available at https://datasheets.raspberrypi.com/rpizero2/raspberry-pi-zero-2-w-product-brief.pdf.

[70] ITU, "Recommendation ITU-r SM.337-4: Separation of frequency and distance." https://www.itu.int/rec/R-REC-SM.337-4-200610-I/en, 10 2006. Accessed: June, 2025.

[71] EnduroSat, "S-band transceiver." https:www.endurosat.com/products/ s-band-transceiver/. Accessed: May 29, 2025.

[72] EnduroSat, "S-band diplexer." https://www.wiran.pl/en/s-band-diplexer. Accessed: May 29, 2025.

[73] R. Corporation, "Rt/duroid® 6006 and 6010.2lm laminates." https: rogerscorp.com/advanced-electronics-solutions/rt-duroid-laminates/ RT-DUROID-6006-AND-6010-2LM-laminates, 6 2025. Accessed: June, 2025.

[74] K. Cheung, "The Role of Margin in Link Design and Optimization," (Piscataway, NJ, United States), Mar. 2015. NTRS Author Affiliations: Jet Propulsion Lab., California Inst. of Tech. NTRS Document ID: 20160009671 NTRS Research Center: Jet Propulsion Laboratory (JPL).

[75] D. Barbaric, J. Vukovic, and D. Babic, "Link budget analysis for a proposed Cubesat Earth observation mission," in *2018 41st International Convention on Information and Communication Technology, Electronics and Microelectronics (MIPRO)*, (Opatija), pp. 0133–0138, IEEE, May 2018.

[76] K. Scheuer, J. Holmes, E. Galyaev, D. Blyth, and R. Alarcon, "Radiation Effects on FR4 Printed Circuit Boards," *IEEE Transactions on Nuclear Science*, vol. 67, pp. 1846–1851, Aug. 2020.

[77] B. N. Bhat, ed., *Aerospace Materials and Applications*. Reston ,VA: American Institute of Aeronautics and Astronautics, Inc., Jan. 2018.

[78] T. A. Association, "Product markets - aircraft and aerospace — aluminium association." https://test-the-aluminum-association.pantheonsite. io/product-markets/aircraft-aerospace.

[79] J. P. Hicks, "Business technology; New materials altering the aircraft industry - the New York Times." https://www.nytimes.com/1989/12/20/business/ business-technology-new-materials-altering-the-aircraft-industry. html, 12 1989.

[80] B. N., "Chapter 2: Aerospace materials characteristics - nasa technical reports server (ntrs)." https://ntrs.nasa.gov/citations/20180001137, August 2018.

[81] MakeItFrom, "6061-t6 aluminum." https://www.makeitfrom.com/ material-properties/6061-T6-Aluminum, 2020.

[82] MakeItFrom.com, "Az91c-t6 magnesium." https://www.makeitfrom.com/ material-properties/AZ91C-T6-Magnesium, 2020.

[83] MakeItFrom, "In ac-43000 (aisi10mg(a)) cast aluminum." https://www.makeitfrom.com/material-properties/ EN-AC-43000-AlSi10Mga-Cast-Aluminum.

[84] E.E. of galvanic coatings, "Sulluge-rich, hard, chromic and black anodized." https://elhco.com/anodizado-duro/, 2023.